

# A low-cost plasma source aimed for medical applications using Ar as the working gas

Fellype do Nascimento<sup>✉</sup>, Bruno Henrique da Silva Leal<sup>✉</sup>,  
Konstantin Georgiev Kostov<sup>✉</sup>

*Faculty of Engineering and Sciences in Guaratinguetá, São Paulo State University–UNESP*

June 23, 2025

## Abstract

Because of the advances in equipment and several studies on medical applications of atmospheric pressure plasmas over the last few years, plasma sources are now being produced for clinical use. It has been demonstrated that plasma sources can be constructed in such a way that their operation and application are safe, and that they present relevant clinical results. However, the manufacturing and operating costs of plasma sources can be decisive for their adoption in medical procedures. In this work, a simple modification of a plasma source that has a low production cost was investigated in order to evaluate the viability of its use for medical applications using argon as the working gas. Without this modification, the plasma source produces high levels of electrical current, which makes it unfeasible for use in medical applications. With the proposed modification, the treatment is no longer carried out using the plasma jet directly, but rather with the post-discharge effluent enriched with reactive oxygen and nitrogen species. As a result, the electrical current reaching the target remains below the safety threshold established for plasma applications in humans. Application tests on water activation indicate that both operating conditions can yield comparable outcomes.

*Keywords:* cold plasma, plasma jet, medical gas plasma, plasma sources

## 1 Introduction

Plasma medicine has become a research field of great interest in recent decades. Advances in equipment intended for medical applications have been quite significant. There are currently products commercially available and, in some cases, certified for medical use by health regulatory agencies in different countries [1, 2, 3, 4]. Most of the plasma sources employed in medical treatments produce cold atmospheric pressure plasmas (CAPPs). The beneficial effects of CAPP treatments are attributed to the reactive oxygen and nitrogen species (RONS) generated within the plasma discharges [5, 6].

CAPPs can be applied to biological targets through two primary methods. One of them is to expose the target to the plasma discharge itself, that is, with the plasma impinging on the target, performing a Direct plasma treatment. The other is with the plasma jet not touching the target, performing an Indirect plasma treatment. Indirect plasma treatment, in turn, can be done with the effluent being directed to the biological sample or via plasma-activated liquids (PAL). The Direct method allows the simultaneous delivery of RONS, UV radiation, and electric fields, which

can induce effects like antimicrobial activity, wound healing, blood coagulation, etc [7, 8]. Indirect treatments through plasma effluent avoids direct electric field effects but is still able to deliver long-lived RONS to biological samples [9]. Plasma-activated liquids, in turn, are able to transfer to the target only those RONS formed by the plasma jet that can be diluted in the treated liquid [10, 11].

Previous researches reported results on Direct plasma treatments in comparison with Indirect treatments using the post-discharge effluent, with both methods being suitable for medical and biomedical applications [12, 13, 14, 15]. Thiyagarajan *et al* applied plasma jets in Direct and Indirect modes on antibiotic resistant bacteria, with better results on bacteria inactivation obtained for the Direct condition [12]. Attri *et al* obtained very similar results in the degradation of dyes for both Direct and Indirect plasma treatments [13]. Lin observed that the pH variation of physiological saline as a function of treatment time is almost the same for both Direct and Indirect plasma exposure [15]. On the other hand, Saadati *et al* reported that the Indirect treatment was not as effective as the Direct method on the treatment of melanoma cancer cells, but the first was found to be less toxic to treated cells [14].

When argon (Ar) is used as the working gas the plasma jets tend to present filamentary patterns. This occurs because the discharge channel becomes highly conductive and very narrow at the same time. Consequently, the resulting plasma jet exhibits higher values of discharge current ( $i_{dis}$ ), gas temperature ( $T_g$ ), and, crucially for medical applications, leakage current, when compared to diffuse discharges. In order to avoid higher  $T_g$  values when operating with Ar some plasma jet devices employ gas flow rates between 5 and 10 slm. However, this solution has some disadvantages like faster dispersion of the RONS. Low  $i_{dis}$  and leakage current values are typically achieved by increasing the distance between the plasma outlet and the target [16, 17]. However, This solution may not work for all cases, especially when Ar is the working gas [18].

A previously reported low-cost plasma source device from our research group is already capable of operating with Ar as the working gas [19]. When configured for Ar, safety parameters like gas temperature and ultraviolet (UV) radiation emission fell within established limits for medical applications. The production of ozone ( $O_3$ ) and nitrogen oxides ( $NO_x$ ) only slightly exceeded those limits. However, the leakage current values significantly surpassed 100  $\mu A$ , which is the value established as safe for applications in human tissues. In this work, a simple modification of the above mentioned device is proposed in order to employ an argon gas flow enriched with RONS formed within the plasma jet for biomedical applications instead of direct application of the plasma jet. In this way, since there is no direct contact between the plasma and the target the  $i_{dis}$  values were shown to be negligible.

## 2 Experimental setup and methods

### 2.1 Plasma source and setup overview

Figure 1 presents an overview of the plasma source (a) as well as a detailed view of the dielectric barrier discharge (DBD) reactor which integrates the device (b). The plasma source comprises a portable power supply and a dielectric barrier discharge (DBD) reactor connected to a 1.0-meter-long flexible plastic tube with outer and inner diameters of 4.0 mm and 2.0 mm, respectively. The DBD reactor features a dielectric enclosure (inner diameter: 10 mm) housing a tungsten pin electrode (diameter: 1.8 mm), which is encased in a closed-end quartz tube with outer and inner

diameters of 4.0 mm and 2.0 mm, respectively. The pin electrode is connected to a male metallic socket, which is mounted onto the dielectric enclosure and connects to the female socket of the power supply. Inside the flexible tube, a thin copper wire (diameter: 0.5 mm) runs along its length, anchored to a metallic connector located within the reactor chamber. The portable power supply, originally modified from a commercial aesthetic treatment device, generates damped-sine waveforms with peak voltages reaching up to 20 kV and an oscillation frequency around 110 kHz. Each damped-sine waveform functions as a high-voltage (HV) burst signal (refer to Fig. 1(b) in [20] for a detailed depiction of the HV waveform). Despite the high-voltage oscillations within each burst, the power supply delivers no more than four pulses per 50 or 60 Hz cycle, depending on the local power grid frequency.

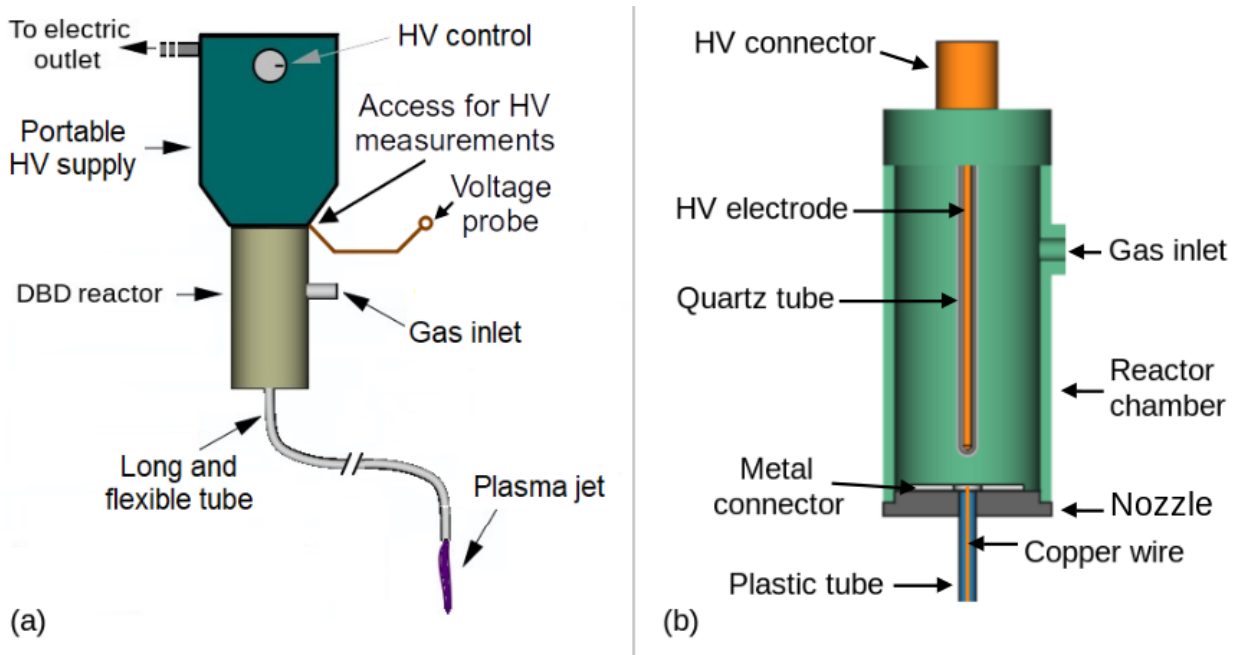


Figure 1: Portable plasma source: (a) overview and (b) details of the DBD reactor.

In this work, a simple modification in the plasma source is proposed in order to allow its use for medical applications using Ar as the working gas. Such modification consists of attaching a 3D-printed spacer (to be referred just as spacer from now on) with a grounded Cu wire, which serves as a target to the plasma jet, to the end of the long tube (see Fig. 2). In this way, the electrical current produced by the plasma discharge does not reach the target. However, the post-discharge effluent continues to carry the long-lived reactive species produced by the plasma jet and can be employed for medical purposes. This can be then called Indirect treatment. Some parameters and properties of plasma jets obtained when operating in Indirect mode were compared to the case when the plasma jet impinges directly on a target (Direct treatment). The schemes used for Direct and Indirect plasma treatments are depicted in Fig. 2. In both cases the spacer was used to constrict the movement of the long tube to the vertical axis only. Although the spacer is not strictly necessary for the Direct plasma jet configuration, it was used (without the Cu wire) to minimize potential differences due to surface wave propagation along the polymer material.

All the parameters and properties of the plasma jets were studied as a function of the distance

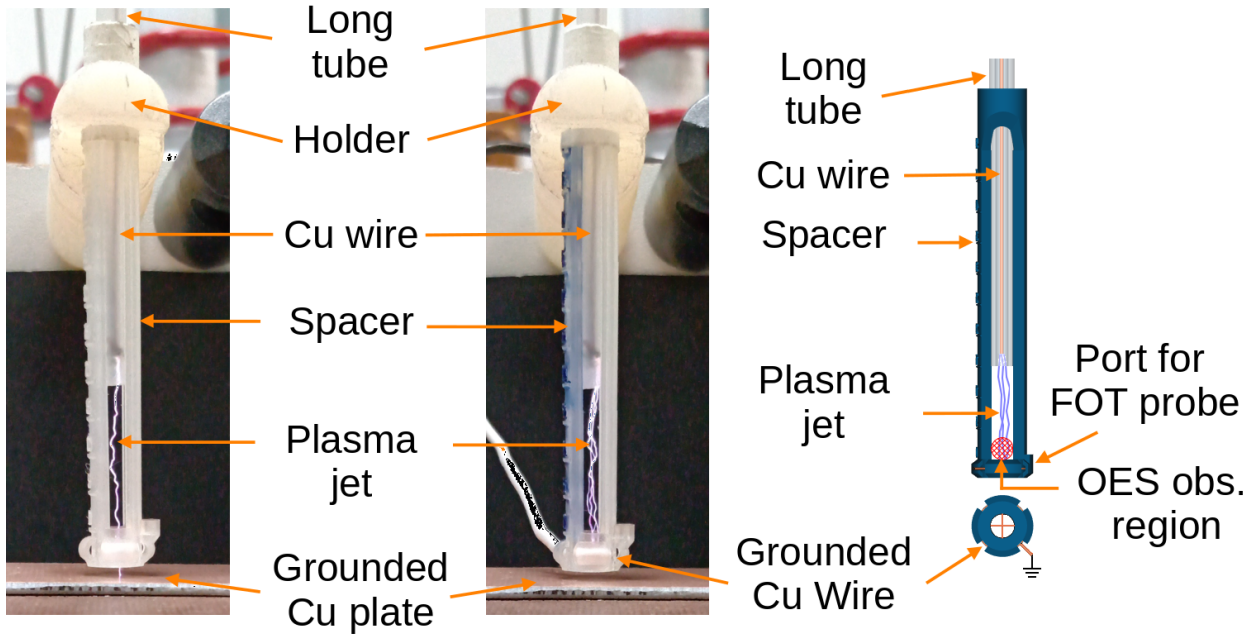


Figure 2: Direct (left) and Indirect (center) setups for plasma treatments and details of the spacer construction (right). The grounded Cu wire is used only in the indirect treatment assembly.

from the plasma outlet and the target. In the Direct treatment, a Cu plate was used as a target for the electrical characterization. For optical emission spectroscopy (OES) characterization, 10 ml of water samples, disposed of on a Petri dish served as the target. The thermal characterization was performed for both the Cu plate and the water as the target. For the Indirect configuration, the target was the Cu wire all the time, but the Cu plate (or a water sample) was always below the spacer. Both the Cu plate and the water samples were placed at a distance of 1 mm from the bottom of the spacer in each case.

The gas flow rate was kept at 2.0 slm for all measurements performed in this work.

## 2.2 Electrical characterization

The electrical characterizations of the device consists mainly of obtaining the discharge power ( $P_{dis}$ ) and effective discharge current ( $i_{dis}$ ) as a function of the distance between the plasma outlet and the target, being that the Cu plate is the target for the plasma jet in the Direct condition while the Cu wire is the target in the Indirect case. For this purpose, the applied voltage ( $V(t)$ ) was measured with a 1000:1 (Tektronix, model P6015A) voltage probe and the voltage across a 47 ohms shunt resistor, placed after the target, was measured to obtain the  $i_{Targ}(t)$  waveform. When operating in the indirect condition, the electrical current at the Cu plate ( $i_{CuP}(t)$ ) was also measured. A 10.0 V/A current monitor (Pearson Electronics Inc., model 8600) was employed for this purpose and these measurements were used to obtain the effective current reaching the Cu plate ( $i_{Cu\ plate}$ ). All the electrical signals were recorded with a four channel oscilloscope (Rigol, model DS1104Z).

The  $P_{dis}$  values were calculated using Eq. (1) [21]:

$$P_{dis} = \frac{1}{\tau} \int_{t_0}^{t_f} v(t) \cdot i(t) dt \quad (1)$$

where  $\tau = 16.67$  ms. And the effective current values ( $i_{RMS}$ ) were calculated as:

$$i_{RMS} = \sqrt{\frac{1}{\tau} \int_0^T i^2(t) dt} \quad (2)$$

### 2.3 Thermal characterization

Measurements of gas temperature ( $T_g$ ) were accomplished by employing a fiber optic temperature (FOT) sensor (Weidmann Technologies Deutschland GmbH, Germany), with 0.2 K precision. When measuring the temperature of the plasma jet, the FOT sensor was placed at the bottom of the spacer, 1 mm above the position for placement of the Cu wire (as indicated in Fig. 2), with its tip always touching the plasma jet. The data acquisition for gas temperature measurements were performed as a function of the distance from outlet to the target – water surface for direct treatment configuration, grounded Cu wire the indirect one. Additionally, the temperature of the effluent only was measured for the Indirect configuration. This was done by placing the FOT sensor tip right below the spacer.

### 2.4 Optical emission spectroscopy characterization

Optical emission spectroscopy was employed for identification of emitting species and for measurements of the intensity of light emitted by selected species. The OES measurements were carried out with the plasma jet impinging on the water surface for the Direct configuration and on the Cu wire for the Indirect one. The light emitted by the plasma jet was collected and conducted to the spectrometer through optical fibers. In this work, the light emitted by the plasma was collected in the region close to the end of the spacer, 2 mm above where the Cu wire would be positioned, as it is highlighted in Fig. 2. A multi-channel spectrometer from Avantes (model AvaSpec-ULS2048X64T), with an instrumental broadening (FWHM) equal to  $0.76 \pm 0.02$  nm was employed to obtain an overview of the emission spectra in the wavelength range from 190 nm to 750 nm. Detailed OES measurements were performed with a multi-channel spectrometer from Horiba (model MicroHR), whose instrumental broadening is  $0.34 \pm 0.01$  nm. The OES measurements made with the Horiba spectrometer were used to extract the intensity of selected species as a function of the distance between the plasma outlet and the water surface. In addition, the Horiba spectrometer was employed for OES measurements in the wavelength range from 730 nm to 840 nm in order to obtain the light emitted by excited oxygen atoms (O I triplet) at 777 nm.

### 2.5 Application in water functionalization

In order to evaluate the amount of reactive species that effectively reach the target upon Direct or Indirect plasma treatment, water samples were exposed to the plasma jet and effluent, respectively. Petri dishes filled with 10 ml of distilled water were placed below the spacer in a way that the distance between the bottom of the spacer and the water surface was nearly 1 mm. The water samples were then exposed to the plasma jet or to the effluent for 3 minutes.

After plasma exposure, the plasma treated water (PTW) samples were analyzed using absorption spectroscopy. For this purpose, an UV–Vis spectrometer from Perkin Elmer (model Lambda25) was employed to obtain absorption curves in the wavelength range from 200 nm to 280 nm. The kind of RONS formed in liquid phase were then investigated by fitting the experimental data with absorbance data of various RONS ( $f_j = f_{RONS_j}$ ) as a function of the wavelength ( $\lambda$ ). The absorbance data were extracted from works that presented absorbance as a function of the wavelength for RONS in aqueous medium [22, 23, 24, 25]. The equation used to perform the curve fitting has the following general form:

$$g(\lambda) = \sum_j m_j f_j(\lambda) \quad (3)$$

where  $m_j$  are multipliers of  $f_j(\lambda)$  and  $g(\lambda)$  is the resulting curve. If the UV-Vis system used to measure the absorption spectrum has absorbance calibration, then the  $m_j$  multipliers return the concentrations of each of the RONS in the plasma treated water [24, 26]. The fitting procedure is done using the Levenberg-Marquardt (*leastsq*) method implemented in the minimize function of the *Lmfit* python package [27]. It finds the  $m_j$  values that minimize the chi-squared ( $X^2$ ) value between the experimental data and the fit curve.

### 3 Results and discussion

#### 3.1 Discharge power and current

Figure 3 displays the curves for discharge power ( $P_{dis}$ ) and effective discharge current ( $i_{dis}$ ) as a function of the distance from gas outlet-to-target ( $h$ ). The curve of effective current at the Cu plate in the Indirect condition ( $i_{Cu\ plate}$ ) as well as its average value are also shown in the graph.

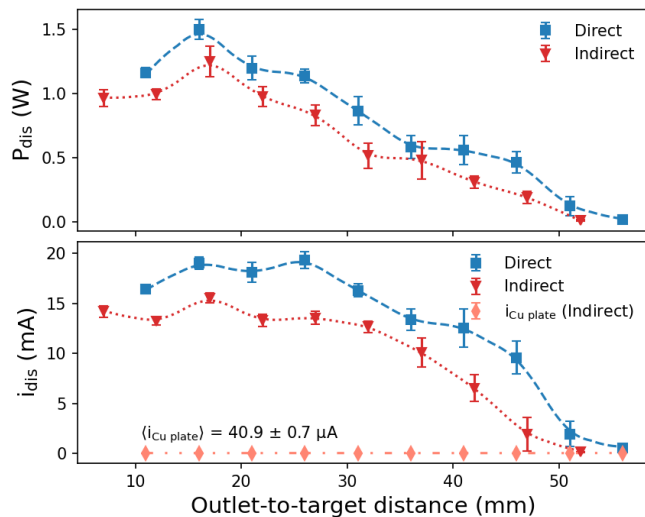


Figure 3: Discharge power (top) and effective discharge current (bottom) as a function of the distance from gas outlet to the first metal target – Cu plate and Cu wire for Direct and Indirect conditions, respectively. The curve of effective current at the Cu plate in the Indirect condition ( $i_{Cu\ plate}$ ) is also plotted in the graph.

From Fig. 3 it can be seen that there are differences in both  $P_{dis}$  and  $i_{dis}$  values when comparing the Direct and Indirect curves. Such differences are possibly related to the accumulation of electrical charges on the surface of the spacer. Since in the direct case the Cu wire is connected to the electrical

ground, the chance of charge accumulation on the polymer surface is much lower than in the Direct case, in which electrical contact between the polymer and electrical grounding is made through plasma discharge.

The values of the  $i_{Cu\ plate}$  as a function of the outlet-to-target distance are almost constant, and its average value is  $40.9 \pm 0.7\ \mu\text{A}$ . This current value is below the value established as safe for devices aimed for medical applications ( $100\ \mu\text{A}$ ). The  $i_{Cu\ plate}$  current is probably related to electrical induction due to the plasma potential added to some electrical charges that are carried by the effluent and reach the Cu plate.

### 3.2 Gas temperature measurements

The results of  $T_g$  measurement as a function of the distance between plasma outlet and target are presented in Fig. 4. As it can be seen, the  $T_g$  values measured with the plasma jet impinging on the water surface (Direct case), are very close to the room temperature, presenting small variations (less than  $1\ ^\circ\text{C}$ ) as the distance from the plasma outlet increases. When operating with the plasma jet impinging on metal targets, in both Direct and Indirect conditions, there are only small differences in the  $T_g$  curves as a function of the outlet-to-target distance. In both cases, the  $T_g$  values start to increase as  $h$  increases, reach a peak temperature near  $h = 30\ \text{mm}$  and then decrease as  $h$  increases.

The differences in the  $T_g$  values with the plasma jets impinging on water or Cu surfaces occur likely because of the large difference in the discharge power achieved for targets with different electrical conductivity values.

In any case, the  $T_g$  values remain significantly lower than the  $40\ ^\circ\text{C}$  threshold, which is the gas temperature limit recommended for medical applications of plasma jets.

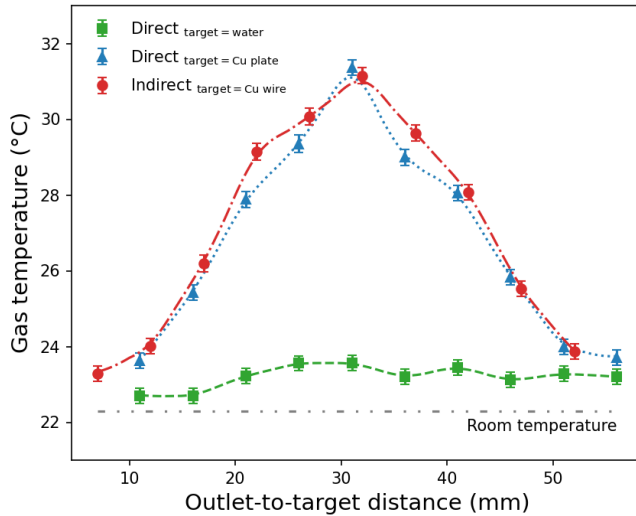


Figure 4: Gas temperature measurements as a function of the outlet-to-target distance for Direct and Indirect conditions. In the Direct case,  $T_g$  was measured with the plasma jet impinging on both water surface (green squares) and Cu plate (blue triangles). In the Indirect case,  $T_g$  was measured with the plasma jet impinging on the Cu wire in the spacer.

### 3.3 Identification of emitting species

Figure 5 displays typical OES spectra measured for the Direct and Indirect configurations. For the Direct case, the spectrum was recorded with the plasma jet impinging on the water surface for an outlet-to-target distance ( $h$ ) equal to 21 mm. In the Indirect case, the plasma jet was impinging

on the Cu wire. Nevertheless, the water sample was kept below the spacer. Thus, the OES measurements were carried out in the same configuration it is used in the assays for applications in water functionalization.

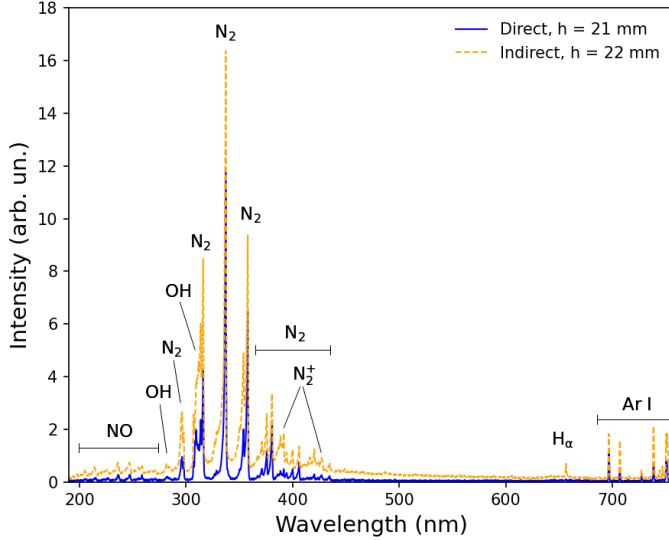


Figure 5: Typical emission spectra of the plasma jets for Direct and Indirect configurations.

From Fig. 5 it can be seen that the excited species in the plasma jet are almost the same, except for the hydrogen emission ( $H_{\alpha}$ ) observed at 656.28 nm. In both cases, the excited molecular species found in the spectra were NO, OH,  $N_2$  and  $N_2^+$ . Line emissions of neutral argon atoms (Ar I) are also present in both spectra, as well as line emissions from neutral oxygen atoms (O I, not shown in Fig. 5, measured with the Horiba spectrometer).

Another visible difference between the spectra recorded for Direct and Indirect configurations is the presence of a continuum emission in the Indirect spectrum, which “lifts up” the spectrum in almost all the wavelength range shown in Fig. 5. This continuum emission is likely due to bremsstrahlung radiation and is mostly linked to collisions among electrons and neutrals in the plasma [28]. It is an indication of higher electron density and temperature values for the plasma jet impinging on the grounded Cu wire, when compared to it impinging on the water.

Although the OES measurements were performed using the same arrangement for both Direct and Indirect conditions, the intensity of the light emitted by the reactive species can not be directly compared because the OES measurements were made at different positions in the plasma column in relation to the target. That is, in the Direct configuration the OES measurements were performed  $\sim 7$  mm above the water surface, while in the Indirect condition the measurements were carried out  $\sim 3$  mm above the Cu wire. In addition, the continuum emission observed in the spectra measured for the Indirect configuration makes the intensity of the reactive species look higher than they really are. However, a qualitative comparison of the intensities as a function of the outlet-to-target distance is still valid and is more relevant for the purposes of this work.

Figure 6 shows the intensities of the light emitted by selected species as a function of the distance from plasma outlet and target (water surface and Cu wire, for Direct and Indirect conditions, respectively). All the measurements presented in Fig. 6 were done using the Horiba spectrometer. From Fig. 6 it can be clearly seen that the behavior of the intensity as a function of  $h$  differs for almost all the curves when comparing Direct and Indirect configurations. The only exception

occurs for OH, for which the curves are very similar, presenting peak values for  $h$  close to 15 mm.

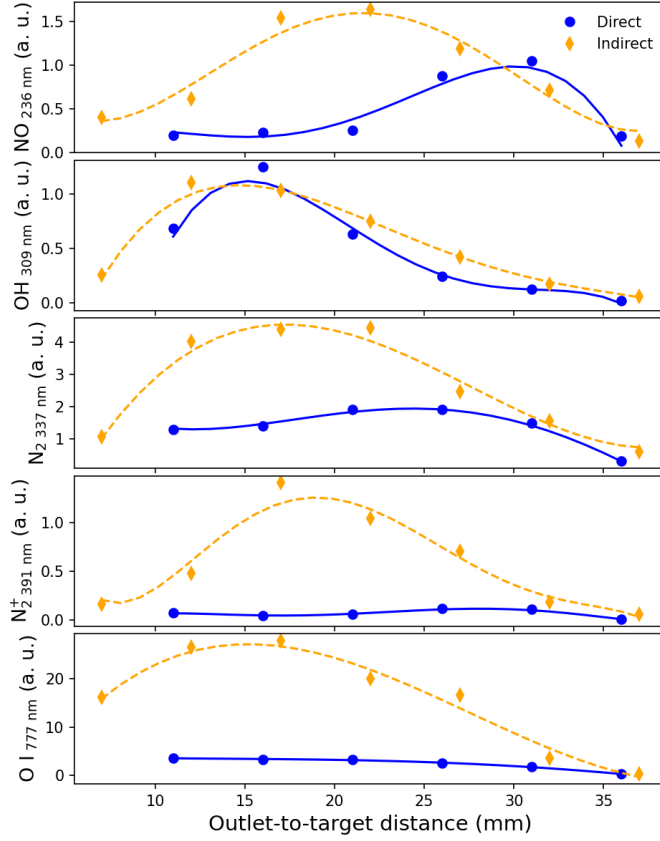


Figure 6: Intensities as a function of the distance between plasma outlet and target for selected reactive species.

Although the intensity values measured under different conditions can not be directly compared, it is worth mentioning that the intensity of O I line emissions measured for the Indirect case are much higher than what was observed for the Direct condition. Since in the wavelength range where the O I emissions are measured the continuum emission from bremsstrahlung radiation is almost negligible, the differences in intensities are then due to the higher density of oxygen atoms in an excited state. Therefore, it can be inferred that the production of oxygen atoms in the Indirect configuration is considerably higher than in the Direct one.

### 3.4 Water treatment results

In this section are presented the results obtained when water samples were exposed to Direct and Indirect plasma treatment. The results of UV-Vis analyses of plasma treated water (PTW) samples are shown in Fig. 7. All the samples in Fig. 7 were exposed to plasma treatment for 3 minutes. In (a) the absorption spectra of all treated samples are presented. In (b), the total absorbance ( $A_{Tot}$  = area under the curve for each sample in (a)) is plotted as a function of the outlet to water distance ( $h_w$ ), comparing the Direct and Indirect operating conditions. The total absorbance of a water sample is related to the amount of RONS retained by the sample after plasma exposure. From Fig. 7(b) it can be seen that the  $A_{Tot}$  values are higher in the Direct case for shorter  $h_w$  values ( $h_w < 20$  mm). However, as  $h_w$  increases, the  $A_{Tot}$  values for the Indirect configuration becomes

higher than the ones for the Direct case, reaching a plateau after  $h_w > 20$  mm.  $A_{Tot}$  presents a decreasing trend as  $h_w$  increases for the Direct configuration.

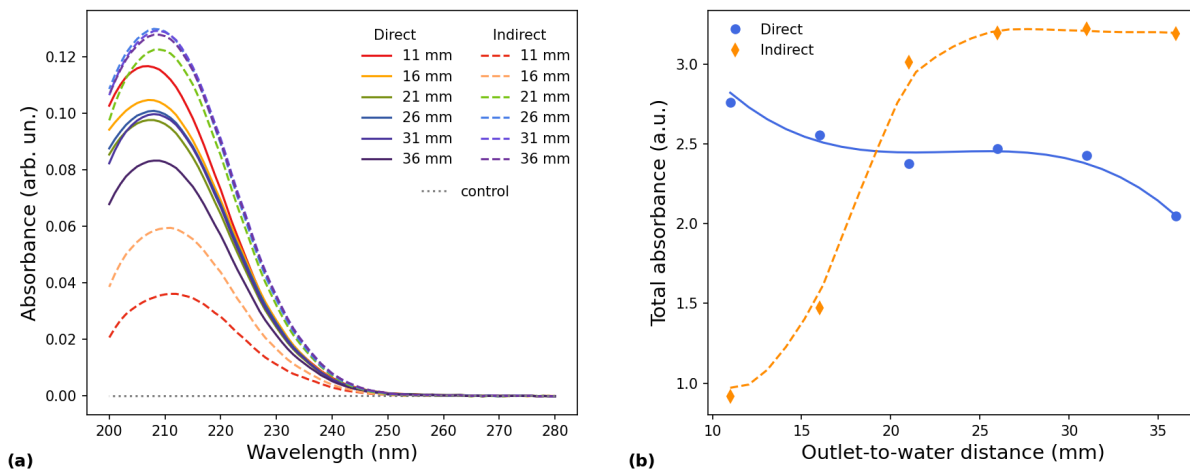


Figure 7: (a) Absorption spectra of water samples exposed Direct and Indirect plasma treatment for various distances from plasma outlet to water surface ( $h_w$ ). (b) Total absorbance as a function of  $h_w$ . The volume of liquid and plasma exposure time were 10 ml and 3 minutes, respectively, for all the samples.

A more detailed analysis of the absorbance spectra shown in Fig. 7(a) was performed for each curve in order to identify the RONS present in the PTW samples. In figure 8 are presented examples of the fitting process for identification of the RONS in the PTW for (a) Direct and (b) Indirect treatment. Figure 9, for instance, presents curves of absorbance by species ( $A_{RONS}$ ) as a function of  $h_w$  for the RONS detected in the PTW samples. The RONS species detected in liquid phase were nitrite ( $\text{NO}_2^-$ ), nitrate ( $\text{NO}_3^-$ ) and, when operating with the Direct configuration, hydrogen peroxide ( $\text{H}_2\text{O}_2$ ). From Fig. 9 it can be seen that  $\text{NO}_2^-$  is the most abundant species detected in the PTW samples, for both operating conditions, followed by  $\text{NO}_3^-$ . A small amount of  $\text{H}_2\text{O}_2$  was detected only in a few water samples exposed to the Direct treatment.

Regarding the operation in the Direct configuration, from Fig. 9 it can be seen that the presence of  $\text{NO}_2^-$  in the water samples does not change significantly among different  $h_w$  values, which probably means that  $\text{NO}_2$  molecules are absorbed by the water in almost the same rate they are produced in the gaseous phase. On the other hand, the amount of  $\text{NO}_3^-$  in the water samples presents a clear decrease trend as  $h_w$  is increased. The  $\text{H}_2\text{O}_2$  for instance, presents a peak value at  $h_w$  equal to 16 mm. However, the amount of  $\text{H}_2\text{O}_2$  detected in the liquid phase is very low, and is probably within the detection limit of the curve fitting performed to identify RONS. This low production of  $\text{H}_2\text{O}_2$  is likely linked to the low exposure time chosen in the experiments.

Regarding the operation in the Indirect condition, the amount of  $\text{NO}_2^-$  detected in the water samples increases relatively fast with  $h_w$  up to 21 mm. And then, the amount of  $\text{NO}_2^-$  remains nearly constant for larger  $h_w$  values. In relation to the  $\text{NO}_3^-$  molecules, they were not detected in the water samples for  $h_w \leq 16$  mm. After that, there is an increment in its production, with a peak value being found at  $h_w = 26$  mm and a small variation to lower values for larger distances of exposure.

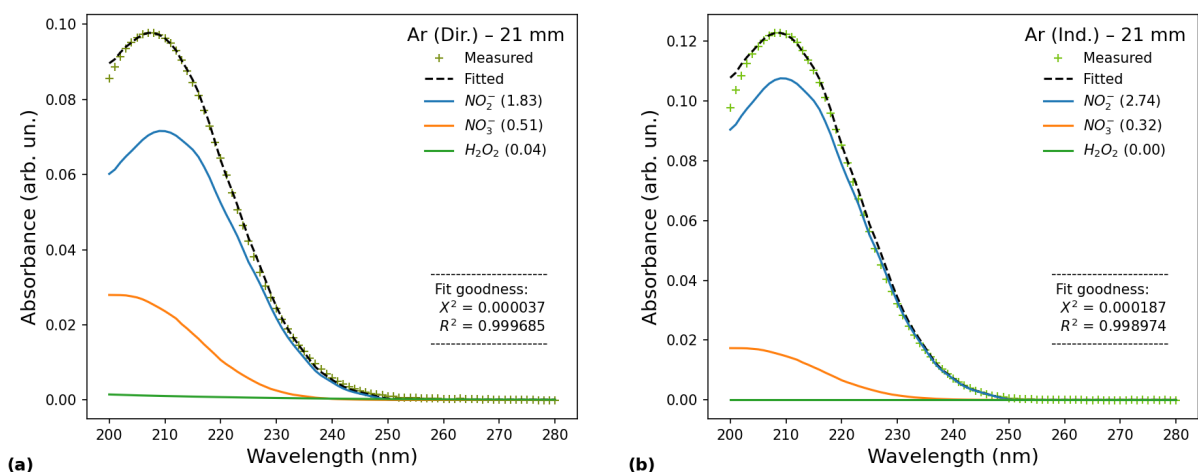


Figure 8: Example of the fitting procedure for RONS quantification in water for (a) Direct and (b) Indirect plasma exposure.

In Fig.10 are presented the results of RONS quantification in water samples exposed to (a) Direct and (b) Indirect treatments for 10 minutes at a distance of 21 mm between the plasma outlet and the water surface. For that distance and exposure time, the total absorbance for the Direct condition is nearly 5% higher than the one obtained for the Indirect case. It can also be seen in Fig. 10 that the production of  $\text{NO}_2^-$  in the water samples was slightly higher for the Indirect exposure and that the production of  $\text{NO}_3^-$  was higher for the Direct treatment. The amount of  $\text{H}_2\text{O}_2$  found in the treated water samples was three times higher using the Direct configuration compared to the Indirect one. Regarding the production of RONS, these data confirms the trend presented in Fig. 9 for  $h_w = 21$  mm. In addition, a small amount of ozone ( $\text{O}_3$ ) was detected only for the Direct case.

A noticeable result shown in Fig. 9 is that the amount of  $\text{H}_2\text{O}_2$  detected in the liquid phase for the Indirect configuration is virtually zero. Considering that the OH production in the gaseous phase (see OES results in Fig. 6) are comparable in both operating conditions (with the caveats already discussed), it would be expected to find  $\text{H}_2\text{O}_2$  in the liquid phase in both conditions (due to the reaction  $\text{OH} + \text{OH} \rightarrow \text{H}_2\text{O}_2$ ), but this has not happened. Nevertheless, since  $\text{H}_2\text{O}_2$  was detected in the water samples treated with both configurations for 10 minutes of plasma exposure, it indicates that just 3 minutes of plasma exposure is not enough for the production of  $\text{H}_2\text{O}_2$  in the liquid phase for the Indirect treatment. These results suggest that the production of  $\text{H}_2\text{O}_2$  occurs preferably in the aqueous phase rather than in the gaseous one. Although this may be a limitation for applications of the Indirect configuration, this fact can be used to selectively produce species in situations where the presence of  $\text{H}_2\text{O}_2$  is undesirable.

Considering only the parameters under variation in this study, a general conclusion comparing the Direct and Indirect operating conditions regarding the production of RONS is that for shorter distances between the plasma outlet and the water surface, it would be better to employ the Direct configuration, while for larger distances the Indirect one would lead to better results.

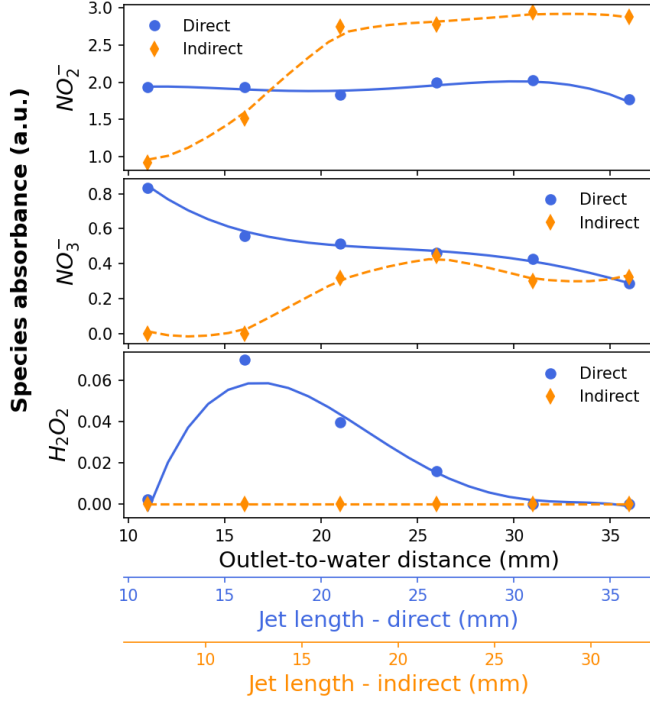


Figure 9: Total absorbance of the detected reactive species as a function of the distance between plasma outlet and water surface. The plasma jet lengths in the Direct and Indirect exposure cases are also indicated in the figure.

## 4 Conclusions

This work aimed to verify whether a small modification in the previously developed plasma device could operate with argon gas safely and with potential for medical applications. The modification in question changed the way in which the plasma treatment would be carried out. The use of the spacer with a copper wire grounded at its bottom meant that the plasma was applied indirectly. Therefore, a comparison with the direct application was necessary. From the electrical results, the discharge power and effective current that reaches the first metal target (Cu plate and Cu wire for Direct and Indirect cases, respectively), are equivalent. However, in the Indirect case, with the copper plate acting as the target of the treatment, as would be a biological target, for example, the electric current that reaches it is much lower than the limit value considered as safe for medical applications of plasmas. From the thermal characterization results, it was found that in all the cases the gas temperature is below the safe operation level (i. e., 40 °C).

Regarding the production of reactive species, from the OES measurements it was found that the production of RONS in the gaseous phase can be considered equivalent for almost all species for both operating conditions. But the production of free oxygen atoms is considerably higher in the Indirect case. For the species detected in the aqueous phase, it was found that it is possible to produce more  $\text{NO}_2^-$  with the Indirect configuration than with the Direct one, with an equivalent production of  $\text{NO}_3^-$  for higher distances between outlet and target. On the other hand, the production of  $\text{H}_2\text{O}_2$  in Indirect applications is usually much lower than what can be achieved with the Direct configuration.

As a general conclusion, from the electrical and thermal characterization results it can be stated that the Indirect configuration offers a safe operating condition, whereas the results from the

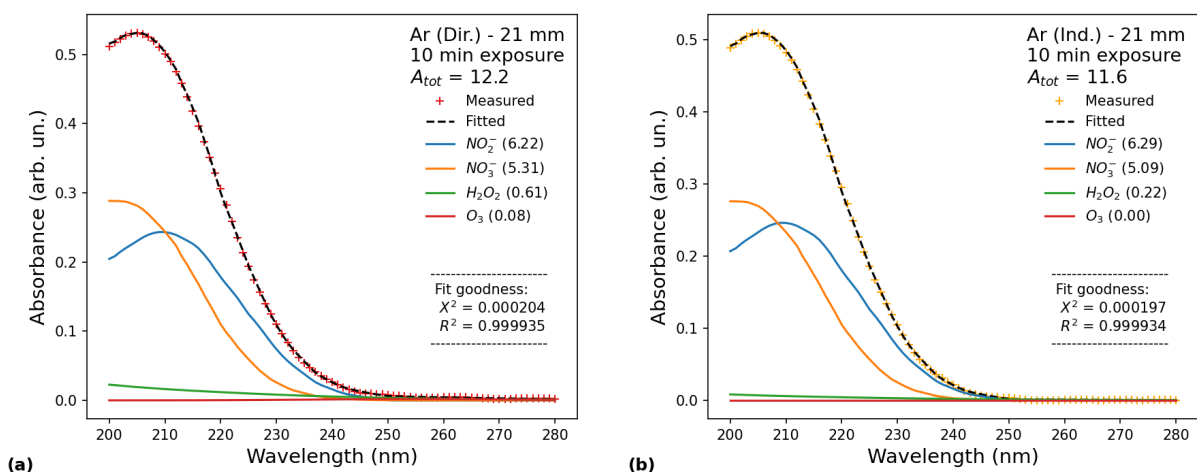


Figure 10: Quantification of RONS in water for (a) Direct and (b) Indirect treatments for 10 minutes of plasma exposure time. The volume of the water samples was 10 ml in both cases.

measurements of RONS, in both gaseous and liquid phases, indicates that the Indirect application produces the elements required for medical applications.

Further studies for optimization of the production of reactive species must be carried out for different gas flow rates as well as for extended exposure times. In addition, the application of the effluent produced by the Indirect configuration must also be done to ensure it has antimicrobial efficacy.

## Data Availability Statement

The data are contained in this manuscript. Raw data are available from the authors under reasonable request.

## Conflict of Interest

The authors declare that there is no conflict of interest in this work.

## Acknowledgments

The authors thank Prof. Dr. Erick Siqueira Guidi for the discussion on the manufacturing of the 3D printed part. This work received financial support from the São Paulo Research Foundation (FAPESP), under Grants #2019/05856-7 and #2020/09481-5, and from Coordination of Superior Level Staff Improvement (CAPES), under Grant #88887.912282/2023-00.

## References

## References

- [1] Simone Duarte and Beatriz H. D. Panariello. Comprehensive biomedical applications of low temperature plasmas. *Archives of Biochemistry and Biophysics*, 693:108560, October 2020.
- [2] Sander Bekeschus, Thomas von Woedtke, Steffen Emmert, and Anke Schmidt. Medical gas plasma-stimulated wound healing: Evidence and mechanisms. *Redox Biology*, 46:102116, October 2021.
- [3] Kolawole Adesina, Ta-Chun Lin, Yue-Wern Huang, Marek Locmelis, and Daoru Han. A Review of Dielectric Barrier Discharge Cold Atmospheric Plasma for Surface Sterilization and Decontamination. *IEEE Transactions on Radiation and Plasma Medical Sciences*, 8(3):295–306, March 2024. Conference Name: IEEE Transactions on Radiation and Plasma Medical Sciences.
- [4] Eun Ji Jeong, Hyun Min Park, Dong Jae Lee, Jun Lee, Jun Yeong Cho, Kyung Deok Seo, Seokjun Je, Min Hyung Jung, Woo Yeon Hwang, and Kyung Sook Kim. Clinical application of cold atmospheric-pressure plasma: mechanisms and irradiation conditions. *J. Phys. D: Appl. Phys.*, 57(37):373001, June 2024. Publisher: IOP Publishing.
- [5] Anna Khlyustova, Cédric Labay, Zdenko Machala, Maria-Pau Ginebra, and Cristina Canal. Important parameters in plasma jets for the production of RONS in liquids for plasma medicine: A brief review. *Front. Chem. Sci. Eng.*, 13(2):238–252, June 2019.
- [6] Cristiane Yumi Koga-Ito, K. G. Kostov, F. S. Miranda, N. V.M. Milhan, N. F. Azevedo Neto, F. Nascimento, and R. S. Pessoa. Cold Atmospheric Plasma as a Therapeutic Tool in Medicine and Dentistry. *Plasma Chem Plasma Process*, 44(3):1393–1429, May 2024.
- [7] Klaus-Dieter Weltmann, Juergen F. Kolb, Marcin Holub, Dirk Uhrlandt, Milan Šimek, Kostya (Ken) Ostrikov, Satoshi Hamaguchi, Uroš Cvelbar, Mirko Černák, Bruce Locke, Alexander Fridman, Pietro Favia, and Kurt Becker. The future for plasma science and technology. *Plasma Processes and Polymers*, 16(1):1800118, 2019. [\\_eprint: https://onlinelibrary.wiley.com/doi/pdf/10.1002/ppap.201800118](https://onlinelibrary.wiley.com/doi/pdf/10.1002/ppap.201800118).
- [8] Mounir Laroussi. Cold Plasma in Medicine and Healthcare: The New Frontier in Low Temperature Plasma Applications. *Front. Phys.*, 8, 2020. Publisher: Frontiers.
- [9] Dezhi Xiao, Cheng Cheng, Yan Lan, Guo Hua Ni, Jie Shen, Yue Dong Meng, and Paul K. Chu. Effects of Atmospheric-Pressure Nonthermal Nitrogen and Air Plasma on Bacteria Inactivation. *IEEE Transactions on Plasma Science*, 44(11):2699–2707, November 2016. Conference Name: IEEE Transactions on Plasma Science.
- [10] Roberto Montalbetti, Zdenko Machala, Matteo Gherardi, and Romolo Laurita. Production and Chemical Composition of Plasma Activated Water: A Systematic Review and Meta-Analysis. *Plasma Processes and Polymers*, 22(1):2400249, 2025. [\\_eprint: https://onlinelibrary.wiley.com/doi/pdf/10.1002/ppap.202400249](https://onlinelibrary.wiley.com/doi/pdf/10.1002/ppap.202400249).

- [11] Pei-Shan Wu, Tzu-Hsuan Wong, Chun-Wei Hou, Teng-Ping Chu, Jyh-Wei Lee, Bih-Show Lou, and Miao-Hsia Lin. Cold Atmospheric Plasma Jet Promotes Wound Healing Through CK2-Coordinated PI3K/AKT and MAPK Signaling Pathways. *Molecular & Cellular Proteomics*, 24(5):100962, May 2025.
- [12] Magesh Thiyagarajan, Abdollah Sarani, and Xavier Gonzalez. Characterization of Portable Resistive Barrier Plasma Jet and Its Direct and Indirect Treatment for Antibiotic Resistant Bacteria and THP-1 Leukemia Cancer Cells. *IEEE Transactions on Plasma Science*, 40(12):3533–3545, December 2012. Conference Name: IEEE Transactions on Plasma Science.
- [13] Pankaj Attri, Maksudbek Yusupov, Ji Hoon Park, Lakshmi Prasanna Lingamdinne, Janardhan Reddy Koduru, Masaharu Shiratani, Eun Ha Choi, and Annemie Bogaerts. Mechanism and comparison of needle-type non-thermal direct and indirect atmospheric pressure plasma jets on the degradation of dyes. *Sci Rep*, 6(1):34419, October 2016.
- [14] Fariba Saadati, Hamed Mahdikia, Hojjat-Allah Abbaszadeh, Mohammad-Amin Abdollahifar, Maryam Sadat Khoramgah, and Babak Shokri. Comparison of Direct and Indirect cold atmospheric-pressure plasma methods in the B16F10 melanoma cancer cells treatment. *Sci Rep*, 8(1):7689, May 2018. Number: 1 Publisher: Nature Publishing Group.
- [15] Yi Tseng Lin. Enhancement of Selected Species in Nonthermal Atmospheric Pressure Plasma: Implications on Wound Healing Effects. *IEEE Transactions on Plasma Science*, 47(2):1134–1144, February 2019. Conference Name: IEEE Transactions on Plasma Science.
- [16] Miriam Stella Mann, Regina Tiede, Karsten Gavenis, Georg Daeschlein, Rene Bussiahn, Klaus-Dieter Weltmann, Steffen Emmert, Thomas von Woedtke, and Raees Ahmed. Introduction to DIN-specification 91315 based on the characterization of the plasma jet kINPen® MED. *Clinical Plasma Medicine*, 4(2):35–45, December 2016.
- [17] Eric Timmermann, Robert Bansenmer, Torsten Gerling, Veronika Hahn, Klaus-Dieter Weltmann, Stefan Nettesheim, and Markus Puff. Piezoelectric-driven plasma pen with multiple nozzles used as a medical device: risk estimation and antimicrobial efficacy. *J. Phys. D: Appl. Phys.*, 54(2):025201, October 2020. Publisher: IOP Publishing.
- [18] Andrei Vasile Nastuta and Torsten Gerling. Cold Atmospheric Pressure Plasma Jet Operated in Ar and He: From Basic Plasma Properties to Vacuum Ultraviolet, Electric Field and Safety Thresholds Measurements in Plasma Medicine. *Applied Sciences*, 12(2):644, January 2022. Number: 2 Publisher: Multidisciplinary Digital Publishing Institute.
- [19] Fellype do Nascimento, Aline da Graça Sampaio, Noala Vicensoto Moreira Milhan, Aline Vidal Lacerda Gontijo, Philipp Mattern, Torsten Gerling, Eric Robert, Cristiane Yumi Koga-Ito, and Konstantin Georgiev Kostov. A Low Cost, Flexible Atmospheric Pressure Plasma Jet Device With Good Antimicrobial Efficiency. *IEEE Transactions on Radiation and Plasma Medical Sciences*, 8(3):307–322, March 2024. Conference Name: IEEE Transactions on Radiation and Plasma Medical Sciences.
- [20] Fellype do Nascimento, Torsten Gerling, and Konstantin Georgiev Kostov. On the gas heating effect of helium atmospheric pressure plasma jet. *Phys. Scr.*, 98(5):055013, April 2023. Publisher: IOP Publishing.

- [21] Andrei V. Pipa and Ronny Brandenburg. The Equivalent Circuit Approach for the Electrical Diagnostics of Dielectric Barrier Discharges: The Classical Theory and Recent Developments. *Atoms*, 7(1):14, March 2019. Number: 1 Publisher: Multidisciplinary Digital Publishing Institute.
- [22] Tan Ling Ling, Musa Ahmad, and Lee Yook Heng. UV-vis spectrophotometric and artificial neural network for estimation of ammonia in aqueous environment using cobalt(II) ions. *Anal. Methods*, 5(23):6709–6714, November 2013. Publisher: The Royal Society of Chemistry.
- [23] Jun-Seok Oh, Hideki Yajima, Keiya Hashida, Tsunehisa Ono, Tatsuo Ishijima, Izumi Serizawa, Hiroshi Furuta, and Akimitsu Hatta. In-situ UV Absorption Spectroscopy for Observing Dissolved Ozone in Water. *Journal of Photopolymer Science and Technology*, 29(3):427–432, 2016.
- [24] Jun-Seok Oh, Endre J. Szili, Kotaro Ogawa, Robert D. Short, Masafumi Ito, Hiroshi Furuta, and Akimitsu Hatta. UV–vis spectroscopy study of plasma-activated water: Dependence of the chemical composition on plasma exposure time and treatment distance. *Jpn. J. Appl. Phys.*, 57(1):0102B9, November 2017. Publisher: IOP Publishing.
- [25] Zhijie Liu, Chunxi Zhou, Dingxin Liu, Tongtong He, Li Guo, Dehui Xu, and Michael G. Kong. Quantifying the concentration and penetration depth of long-lived RONS in plasma-activated water by UV absorption spectroscopy. *AIP Advances*, 9(1):015014, January 2019.
- [26] J Petković, R van de Wege, J R Wubs, O J A P van Rooij, J J van Oorschot, T Huiskamp, and A Sobota. Assessment of reactive species concentrations in plasma-treated water: a pH and conductivity-based method validated by absorption spectroscopy. *J. Phys. D: Appl. Phys.*, 57(23):235202, March 2024. Publisher: IOP Publishing.
- [27] Matthew Newville, Till Stensitzki, Daniel B. Allen, Michal Rawlik, Antonino Ingargiola, and Andrew Nelson. Lmfit: Non-Linear Least-Square Minimization and Curve-Fitting for Python. *Astrophysics Source Code Library*, page ascl:1606.014, June 2016. ADS Bibcode: 2016ascl.soft06014N.
- [28] Sanghoo Park, Wonho Choe, Holak Kim, and Joo Young Park. Continuum emission-based electron diagnostics for atmospheric pressure plasmas and characteristics of nanosecond-pulsed argon plasma jets. *Plasma Sources Sci. Technol.*, 24(3):034003, April 2015. Publisher: IOP Publishing.